A physics-based correction model for homogenizing sub-daily temperature series

R. Auchmann[1] and S. Brönnimann[1]

Received 7 May 2012; revised 31 July 2012; accepted 6 August 2012; published 15 September 2012.

[1] A new physics-based technique for correcting inhomogeneities present in sub-daily temperature records is proposed. The approach accounts for changes in the sensor-shield characteristics that affect the energy balance dependent on ambient weather conditions (radiation, wind). An empirical model is formulated that reflects the main atmospheric processes and can be used in the correction step of a homogenization procedure. The model accounts for short- and long-wave radiation fluxes (including a snow cover component for albedo calculation) of a measurement system, such as a radiation shield. One part of the flux is further modulated by ventilation. The model requires only cloud cover and wind speed for each day, but detailed site-specific information is necessary. The final model has three free parameters, one of which is a constant offset. The three parameters can be determined, e.g., using the mean offsets for three observation times. The model is developed using the example of the change from the Wild screen to the Stevenson screen in the temperature record of Basel, Switzerland, in 1966. It is evaluated based on parallel measurements of both systems during a sub-period at this location, which were discovered during the writing of this paper. The model can be used in the correction step of homogenization to distribute a known mean step-size to every single measurement, thus providing a reasonable alternative correction procedure for high-resolution historical climate series. It also constitutes an error model, which may be applied, e.g., in data assimilation approaches.

Citation: Auchmann, R., and S. Brönnimann (2012), A physics-based correction model for homogenizing sub-daily temperature series, *J. Geophys. Res.*, *117*, D17119, doi:10.1029/2012JD018067.

1. Introduction

[2] Homogenized long-term climatological time series provide useful information on climate back to the preindustrial era. In recent years, climate extremes have come into focus, and consequently, homogeneous meteorological records are required in high temporal resolution [*Moberg et al.*, 2000; *Brandsma and Können*, 2006]. The number of such data sets is increasing, but still rare compared to monthly [*Venema et al.*, 2012] or annually resolved data [*Moberg et al.*, 2006]. Moreover, the homogenization of daily or sub-daily data is different from the homogenization of monthly or annual data as the former involves dealing with non-linear atmospheric processes that influence the distribution [*Della-Marta and Wanner*, 2006]. Homogenization of daily and sub-daily data has been challenged only in recent years [*Aguilar et al.*, 2008]. In this paper, we propose a correction method for temperature that can be applied to sub-daily data. Existing methods correcting for daily or sub-daily temperature data can be grouped into three basic categories:

[3] 1. Corrections of the mean: Methods that start from monthly mean break sizes, which are then distributed to individual days. Daily corrections are computed by fitting a spline or piecewise linear function between monthly mean corrections that are preserved [*Vincent et al.*, 2002; *Begert et al.*, 2003].

[4] 2. Corrections of higher-order moments of the distribution: Methods that directly adjust the distribution of daily temperature based on a daily reference series [*Della-Marta and Wanner*, 2006; *Štěpánek et al.*, 2009; *Toreti et al.*, 2010; *Mestre et al.*, 2011]. The correction thus depends on the temperature itself.

[5] 3. Methods that incorporate basic physics such as the effects of radiation and ventilation on the temperature shield [*Z'graggen*, 2006].

[6] In addition, mixed approaches are possible. For instance, by making corrections dependent on weather types or similar, some physical causes for inhomogeneities are admitted, although not explicitly. While statistical corrections often deal with temperature statistics ($mean_{day}(T)$, $\min_{day}(T)$, $\max_{day}(T)$), physics-based correction methods require state observations $T(t)$ because ambient conditions need to be known for the

[1]Institute of Geography and Oeschger Center for Climate Change Research, University of Bern, Bern, Switzerland.

Corresponding author: R. Auchmann, Institute of Geography and Oeschger Center for Climate Change Research, University of Bern, Hallerstrasse 12, CH-3012 Bern, Switzerland. (renate.auchmann@giub.unibe.ch)

0148-0227/12/2012JD018067

Figure 1. (left) The Wild screen is a metallic screen, open to the north and the bottom. (right) The smaller, wooden Stevenson screen is closed on all sides and has a double roof and louver walls, with much smaller blinds than for the Wild screen. (Pictures by P. Della-Marta.)

time of observation (which is not known e.g. for $\max_{day}(T)$). Ideally, the corrections then do not depend on reference series anymore, but only on the physics, presuming at least a crude understanding of the error. Inhomogeneities, for example, caused by a change in measurement systems, vary with solar radiation [*Peterson et al.*, 1998] and ambient wind speed [*Hubbard et al.*, 2001; *Lin et al.*, 2001; *Lin and Hubbard*, 2001]. Former studies on naturally or poorly ventilated thermometer screens and intercomparisons among different sensor-shield systems [*Guttman and Baker*, 1996; *Richardson et al.*, 1999; *Hubbard et al.*, 2001; *Lin et al.*, 2001; *Lin and Hubbard*, 2001; *Nakamura*, 2005; *van der Meulen and Brandsma*, 2008; *Brandsma and van der Meulen*, 2008; *Huwald et al.*, 2009; *Harrison*, 2010] show that radiative heating during daytime, IR cooling during nighttime, cloud cover, ground albedo, and wind speed are the main factors that influence the magnitude and sign of the error. *Lin and Hubbard* [2001] find first that radiative heating during daytime leads to the largest bias magnitudes. Low ambient wind speeds support this tendency [*Nakamura*, 2005; *Harrison*, 2010; *Lin et al.*, 2001]. This can lead to differences between air temperature within the shield and outside a radiation shield, which may reach −0.5°C to 2.5°C [*World Meteorological Organization*, 2008]. Second, in accordance with *Nakamura* [2005], *Lin and Hubbard* [2001] found a non-linear relationship between the ambient wind speed and the magnitude of the bias. Accordingly, including information on at least these two main well-known causes for biases in the correction procedure may result in more realistic correction magnitudes for sub-daily temperature values and in fact may be a more straightforward way to correct inhomogeneities.

[7] Thus far, the only physics-based correction method that uses radiation and wind speed was published by *Z'graggen* [2006] and applied to daily maximum temperature data. *Z'graggen* [2006] uses monthly mean parameterized maximum global irradiance at one location depending on cloud cover and uses the long-wave radiation balance together with daily wind speed measurements as a basis for his correction. The days of a month with the same wind speed and mean radiation balance are assigned equal correction magnitudes (which allows the application to daily maximum data). However, in months with a steep annual radiation cycle this assumption may not be appropriate over a month.

[8] In this paper, we present the background and development of an advanced semi-empirical, physics-based correction procedure for adjusting sub-daily temperature series starting from *Z'graggen*'s [2006] central idea. Our procedure is based on a simple energy balance model of a screen that accounts for screen and sensor geometry, net radiation at the surface of the screen (including short- and long-wave components and a snow-accumulation model for deriving albedo), and the modification of the sensible heat flux between the screen and the sensor through wind speed (ventilation). As the target of the correction is not to adjust the observed air temperature to the (unknown) true air temperature, but to adjust for differences between two systems, the model is applied to the difference between two sensor-screen systems, additionally accounting for a possible instrument offset. The approach has three parameters that need to be known or estimated, but highly correlated sub-daily, daily, monthly, or annual reference series are necessary at this step. If the three parameters are estimated from the mean break sizes determined for three observation times (morning, evening, noon), the approach will preserve the mean shift but redistribute it to single measurements based on physics. In this paper, we apply our method to an inhomogeneity in the Basel temperature series that occurred in 1966 due to a change in radiation shields (Station-history Basel, MeteoSwiss Archive). Thus, the impact is assessed on a sub-daily basis, for a specific cause of inhomogeneity, which is supposed to deliver more realistic and accurate results [*Vincent et al.*, 2002].

[9] This article proceeds as follows. In Section 2, we describe data we use for our radiation and correction model. We show the development of the correction model, including the radiation and snow-accumulation model, in Section 3. We present and discuss an evaluation of the resulting corrections using parallel measurements and the impact on extremes in Section 4. Concluding remarks are drawn in Section 5.

2. Data

[10] In this study, we use sub-daily temperature series from 1956 to 1970 from Basel-Binningen, situated in the north of Switzerland (47° 33′N, 7° 35′E), at 316 m a.m.s.l. During the 1956–1970 period, temperature measurements were taken three times daily, at 6:00, 12:00, and 20:00 UTC with a ventilated psychrometer. Throughout this paper, times will be given in UTC unless otherwise noted. This period starts in 1956 because before 1956 a liquid-in-glass thermometer was used. The period ends in 1970 as afterwards the evening observation time was changed from 20:00 to 18:00. Until 1966, a Wild screen (Figure 1, left) served as radiation shelter, and in 1966 the Wild screen was replaced by a Stevenson screen (Figure 1, right) (Station-history Basel, MeteoSwiss Archive), which caused an inhomogeneity. In the following, we refer to the homogeneous subperiod before the break (1956–1965) as *H*2 and to the period after the break (1966–1970) as *H*1.

[11] From 1957 to 1962 (referred to as *H*3), simultaneous temperature measurements were performed in the Wild and the Stevenson screen (see Figure 2). We recently discovered

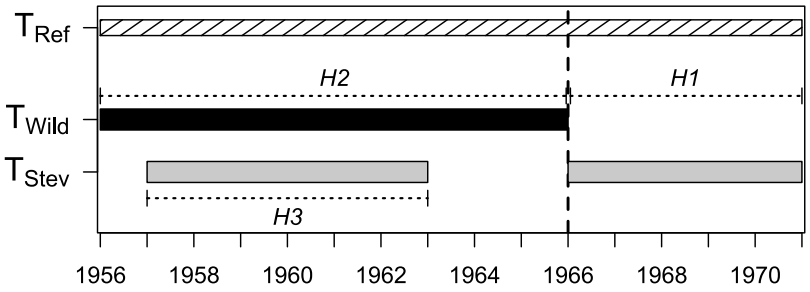

Figure 2. Overview of the homogeneous subperiods and temperature records used in this study, T_{Stev}, T_{Wild}, and T_{Ref}, denoting temperature measurements taken in Basel-Binningen in the Stevenson screen and in the Wild screen, and the reference station (Zurich), respectively. $H1$ is the most recent period from 1966–1970, $H2$ denotes the period before the break 1956–1965 (period, which is going to be homogenized), and $H3$ denotes the period 1957–1962, when parallel temperature measurements where performed in the Wild and the Stevenson screen. The dashed vertical line marks the time of the inhomogeneity, 1966, the timing of the change from the Wild to the Stevenson screen.

(in the Archive of the Meteorologischer Verein in Basel) and digitized the parallel measurements taken in the Stevenson screen ($T_{Stev\ H3}$) from the original handwritten observation books. The $T_{Stev\ H3}$ morning and noon measurements were taken at the same time as the T_{Wild} measurements; the evening observation times occasionally differed, but the time was noted. We excluded evening measurements from $T_{Stev\ H3}$ that were taken more than half an hour before or after 20:00. We further excluded eight outliers, which differ more than 3°C from T_{Wild}. The occurrence of the outliers shows no systematic behavior; they occur throughout the year at different temperatures. The original record revealed ambiguous handwriting for the outliers. From different archives (MeteoSwiss, Meteorologischer Verein Basel), we collected all metadata available for Basel-Binningen to confirm the inhomogeneity on 1 January 1966 and to confirm that there were no further changes in our period of interest ($H2 + H1$), which was also shown by *Begert et al.* [2005] and *Kuglitsch et al.* [2012]. Hence, the overall period 1956–1970 comprises only one inhomogeneity, which is the target of our study. The sub-periods before, $H2$, and after the break, $H1$, are considered homogeneous and sufficiently long for determining the break size.

[12] As input for the radiation model, we use sub-daily wind speed (original Beaufort units converted to m/s), relative humidity (%), precipitation (*mm*), and cloud cover (*octas*) series from Basel-Binningen, taken at the three observation times in the period 1956–1970. Wind speed was observed (not measured) and given in Beaufort categories. Furthermore, snow height data (cm) are used to evaluate the modeled dates of snow cover from our snow-accumulation model. From the Basel-Binningen station history, we extracted information on the geometry of the observation site (local horizon for possible shading effects from buildings, for example) in our period of interest as well as times of the local sunrise and sunset over a one year period.

3. Methods

3.1. Energy Balance of the Screen-Sensor System

[13] Our approach is similar to a simple energy balance model of the screen-sensor system. One term basically represents the heating of the screen, which is assumed to be proportional to the net radiation incident on its surface (R_2). The approach assumes that heat may reach the sensor in two ways, either as radiative flux from the screen or from the atmosphere (depending on the screen geometry), R_1, or as sensible heat flux from the screen, $Q_{sensible}$. However, due to the strongly linked relation of the two fluxes a clear separation and separate calculation is not possible. We further assume one part of the flux is mostly independent from wind speed (R_1) and the other part of the flux is further modulated by wind speed ($Q_{sensible} = R_2 * f(v)$, see Section 3.3). We express the heating of the sensor (Q_{sensor}) in any sensor-shield system as a combination of the two radiation terms as

$$dQ_{sensor} = c_1 * R_1 + c_2 * Q_{sensible} = c_1 * R_1 + c_2 * R_2 * f(v), \quad (1)$$

with c_1 and c_2 representing coefficients. The unequal screen geometries of the Wild and Stevenson screens result in unequal radiative-shielding characteristics [*Müller*, 1984; *Nordli et al.*, 1997; *Begert et al.*, 2005]. In contrast to the Stevenson screen, the Wild screen is open to the north and has no bottom, while the Stevenson screen is closed on all sides and has smaller blinds (Figure 1). Hence, the sensor in the Wild screen is directly exposed to radiative flux from the atmosphere; however, sensible heat flux from the screen may be decreased due to better natural ventilation. This leads to differing heating of the sensors, $Q_{sensor1} \neq Q_{sensor2}$ under equal meteorological conditions.

3.2. Radiative Balance Model and Snow-Accumulation Model

[14] In a next step, we approximate R_1 and R_2 separately. Information on screen geometry in addition to high temporal resolution meteorological data allows radiative fluxes to and from an object to be approximated using a simplified set of equations. In the short-wave range, we separately address direct and diffuse radiation from the atmosphere and reflected radiation from the ground. In the long-wave range we separately account for downward counter-radiation from the atmosphere and from clouds as well as upward thermal radiation from the ground.

[15] However, several assumptions are needed to approximate the fluxes due to a lack of radiation flux measurements and detailed information on cloud cover. Important

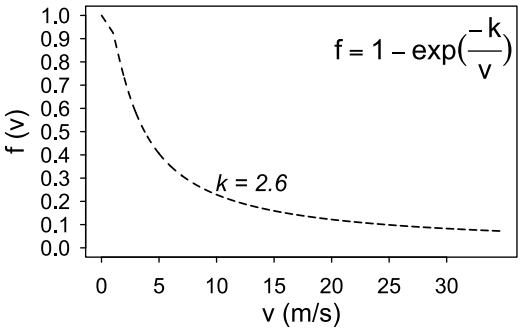

Figure 3. Wind attenuation term f for $k = 2.6$.

parameterizations and assumptions for some of the components are detailed in the following; for a complete description and parameterization of all components, the reader is referred to Appendix A.

[16] To derive direct radiation S_p (equation (A3)), for cloudy conditions we assume a linear relationship between S_p and cloud cover fraction. Under cloudy conditions, uncertainties increase due to a lack of information on the relative position of the sun to the clouds and cloud properties. The transmissivity of the atmosphere (τ) for clear sky conditions is set to a value of 0.75 [*Gates*, 1980].

[17] Computing the fraction of sky diffuse radiation S_d, especially for cloud-covered conditions, is more complex. It depends on the albedo of the ground, the height and type of clouds, the number and size of particles in the atmosphere, and the position of the sun relative to the clouds [*Campbell and Norman*, 1998]. Diffuse radiation under clouds is usually one magnitude smaller than global radiation under clear sky conditions and strongly correlated with direct short-wave radiation [*Paltridge and Platt*, 1976]. However, the relative amount of diffuse radiation compared to direct radiation rises as the cloud cover increases [*Gates*, 1980]. For calculating S_d, we adapt an empirical equation from *Liu and Jordan* [1960] (equation (A5)). For non-clear days we use a cloud modification factor *cmf*, which attenuates τ. We calculate *cmf* by linearly interpolating between 0.3 (fully covered) and 0.75 for fractional cloud cover c, from zero to one, being aware that this is only a rough approximation. Thus, the relation of τ and c for calculating diffuse radiation is not necessarily linear, as expressed by the application of the *cmf* in equation (A5). However, our information on clouds is limited to the cloud cover fraction only.

[18] For calculating incoming thermal radiation from the atmosphere L_a, we separately account for the cloud-covered and the cloud-free fraction of the sky ($L_a = L_{a,clear} + L_{a,covered}$). We use the Stefan-Boltzmann relationship to estimate the downward long-wave counter radiation from the clear fraction of the sky $L_{a,clear}$ (equation (A9)). For describing the emissivity of the atmosphere ϵ_a, we use the parametrization of *Brutsaert* [1975] (equation (A10)). For the cloud-covered fraction of the sky, we use the emissivity of clouds ϵ_c in the Stefan-Boltzmann relationship instead of ϵ_a, as well as cloud base temperature, T_c, instead of air temperature near the ground T_a. To describe T_c, we calculate the temperature at the lifting condensation level [*Bolton*, 1980; *Corti and Peter*, 2009]. For ϵ_c, we use the relationship proposed by *Stephens et al.* [1990], $\epsilon_c = 1 - e^{0.75\tau_{clouds}}$, where the wavelength-dependent optical depth, τ_{clouds}, was parameterized by the short-wave optical depth for low cumulus clouds, and taken as 0.95 [*Paltridge and Platt*, 1976].

[19] For thermal radiation emitted from the ground L_g, we also use the Stefan-Boltzmann relationship. Since no ground temperature measurements were available, we use the actual measured temperature T_a to approximate the ground temperature for days without snow cover. For snow covered days, we use a constant ground temperature of −2°C.

[20] We apply sky view factors [*Oke*, 1987; *Campbell and Norman*, 1998] to account for the portion of the sky or ground (source of radiation) to which the sensor or the screen surface is exposed for a given screen geometry. A detailed description of the view factors is provided at the end of Appendix A.

[21] Short-wave radiation flux is strongly influenced by ground albedo [*Huwald et al.*, 2009], which in turn changes heavily with the presence of snow [*Bonan*, 2002]. To account for changing ground albedo, snow cover data are required. Since such data are rare, we implied a snow-accumulation model based on the degree-day method [*Singh and Singh*, 2001], resulting in daily ground albedo values. A detailed description of the model and the parameterizations is given in Appendix B.

3.3. Sensible Heat Flux

[22] Screen design heavily influences ventilation characteristics of a sensor-shield system. A consequence of the Wild screen open to one side is the better ventilation of the sensor due to enhanced convective heat exchange and mixing of ambient air with air within the shield [*Lin et al.*, 2001]. Thus, ventilation can counteract a bias produced by an overheating of the screen surface due to an uncoupling of the air inside the shield from the ambient air. We introduce an attenuation term ($f(v)$ in equation (1)) that modulates the sensible heat flux component (or net radiation incident on the screen surface). At increasing wind speeds, the heat transfer rate due to convection is exponentially decreasing [*Lin and Hubbard*, 2001], and therefore sensible heat flux from the screen approaches asymptotically zero [*Z'graggen*, 2006]. We hence derive the following attenuation term $f(v)$:

$$f = 1 - \exp\left(\frac{-k}{v}\right), \tag{2}$$

where v is the wind speed and k is a coefficient. We adopt k in a way that the shape of the curve follows the formulation suggested by *Väisälä* [1941, 1949] and *Raunio* [1950] (further applied by *Brönnimann* [2003]), and physical plausible model parameter estimates ($c_1 < 0$ and $c_2 < 0$, see equation (1)) can be derived. We achieve this by assigning a value of $k = 2.6$. For wind speeds <6 m/s (comprising 99.2 % of all wind speed observations), the derived shape (see Figure 3) follows the shape of *Väisälä* [1941, 1949] and yields the assumed negative parameter signs. Within the range of 6 m/s to 34 m/s (comprising the remaining 0.8 % of wind speed observations), the shape of the *Väisälä* [1941, 1949] curve and our derived curve deviate only slightly (not shown). We therefore use the same k for all wind speeds. Note, deriving a physical relationship is hardly possible as

Table 1. Mean Differences ($\overline{\Delta s_j}$) Derived From the Parallel Measurements ($\overline{\Delta p_{i\in H3\ j}}$) and Statistically Estimated Mean Differences ($\overline{\Delta r_{i\in H2\ j}}$) From a Reference Series for the Three Observation Times j

j	$\overline{\Delta p_{i\in H3}}$	$\overline{\Delta r_{i\in H2}}$
Morning	0.11	0.14
Noon	−0.32	−0.41
Evening	0.40	0.45

wind speed was observed (not measured) and is given in Beaufort categories.

3.4. Correction Model

[23] Correction approaches in homogenization do not correct for differences between a measured temperature series and the (unknown) true air temperature, but for non-climatic differences between two series (in our case two sensor-screen set-ups). For the temperature difference between the two set-ups, we assume that equation (1) can be used, with the addition of a constant.

[24] In other words, we assume that the heating in the later set-up, to which the earlier is adjusted, can be expressed in the same way as the earlier, so that the desired coefficients are simply the differences of two coefficients. Additionally, a constant offset Δc_0 needs to be introduced as changes in the set-up are often accompanied by further changes e.g. in the instrument.

$$\Delta e = \Delta c_0 + \Delta c_1 * R_1 + \Delta c_2 * R_2 * \left(1 - \exp\left(\frac{-k}{v}\right)\right), \quad (3)$$

with Δe being the temperature difference between the two set-ups. The three coefficients can be estimated by using three sufficiently different constraints, as will be detailed in the next subsection. In some cases, the coefficients may also be known, or they may be taken from estimations from similar cases (e.g., Δc_1 and Δc_2 may be characteristic for the change from the Wild screen to the Stevenson screen and thus applicable to other cases, although site-specific conditions may still play a role).

[25] We use the mean differences ($\overline{\Delta s_j}$) for each of the three observation times j, averaged over all days i of the period under consideration, to constrain the coefficients. This results in a system of three linear equations of the form

$$\overline{\Delta s_j} = \Delta c_0 + \sum_{i=1}^{n} \Delta c_1 * R_{1\ i,j} + \sum_{i=1}^{n} \Delta c_2 * R_{2\ i,j} * \left(1 - \exp\left(\frac{-k}{v_{i,j}}\right)\right), \quad (4)$$

which can be solved. As the determined coefficients represent characteristics of the measurement system, we regard them as constant for all observation times throughout a period of unchanged installation and instruments. Using the coefficients, corrections can be calculated for any weather situation. However, the transferability of the coefficients to other breaks (e.g., within the same climatic region) needs to be explored. Every single temperature value receives an individual correction based on the ambient weather conditions. At the same time, the mean step sizes (the constraints) are preserved. The method thus simply redistributes the mean error in a physically plausible way. The knowledge of the mean step size is sufficient and only the annual reference series is required. Additional constraints, combined with statistical estimations, might alternatively be used.

3.5. Systematic Application of the Model and Calculation of Step-Sizes

[26] We use two different ways to estimate $\overline{\Delta s_j}$. First, we derive $\overline{\Delta s_j}$ from the parallel measurements, termed $\overline{\Delta p_j}$. Using the "true" differences allows an assessment of the properties of the error model. Second, we use statistically estimated differences ($\overline{\Delta r_j}$) with a reference series in a longer period ($H2$, see Figure 2). This is a more realistic approach, but folds additional uncertainty (which is not due to our error model) into the results. To select an adequate reference series for deriving $\overline{\Delta r_j}$, we computed correlations with several nearby Swiss stations and subsequently consulted their detailed station histories for any changes in the period 1956–1970. We applied the method proposed by *Peterson and Easterling* [1994] to deseasonalized monthly mean series and found the station Zurich to be the highest correlated series without documented changes in our period of interest. The correlation coefficients for the morning, noon, and evening series yield 0.98 (1956–1970) for all three series.

[27] In a first step, we derive corrections in $H3$, the period of parallel measurements, and use the mean $\overline{\Delta p_j}$ values (one for each of the three observation times) as constraints of equation (4) with

$$\overline{\Delta s_j} = \overline{\Delta p_j} = \overline{T_{Stev\ i\in H3\ j} - T_{Wild\ i\in H3\ j}}, \quad (5)$$

Corrections derived in this way are termed $\Delta e_{p\ ij}$.

[28] In the process of homogenization, the most recent period is assumed to provide the most realistic values regarding the true values, where the true value, however, is not known. Hence, in the next step we correct the latter period, $H2$ regarding the most recent period, $H1$. Alternatively, we constrain our correction model using the reference series with

$$\overline{\Delta s_j} = \overline{\Delta r_j} = \overline{\left(T_{Ref\ i\in H2\ j} - T_{Wild\ i\in H2\ j}\right)} - \overline{\left(T_{Ref\ i\in H1\ j} - T_{Stev\ i\in H1\ j}\right)}, \quad (6)$$

Corrections derived in this way are termed $\Delta e_{r\ ij}$.

[29] Table 1 presents the mean differences for $\overline{\Delta p_j}$ and $\overline{\Delta r_j}$ for the morning, noon, and evening temperature series. For $\overline{\Delta r_j}$, we find a negative mean shift for the noon series (−0.41°C), and positive mean shifts for the morning and evening series (+0.14°C and +0.45°C, respectively), suggesting the Stevenson screen has more effective radiation sheltering characteristics. Similar mean differences are found for $\overline{\Delta p_j}$.

4. Results and Discussion

4.1. Comparison of Physics-Based Corrections With Parallel Measurements

[30] Constraining equation (4) with $\overline{\Delta p_j}$ yields the model parameters given in the first column of Table 2. In Figure 4,

Table 2. Estimated Model Parameters

	$\overline{\Delta s_j} = \overline{\Delta p_{i\in H3\ j}}$	$\overline{\Delta s_j} = \overline{\Delta r_{i\in H2\ j}}$
Δc_0	0.248	0.809
Δc_1	−0.000034	−0.0017
Δc_2	−0.0115	−0.0116

the corrections $\Delta e_{p\ i\in H3\ j}$ are compared to $\Delta p_{i\in H3\ j}$ in the period 1957–1962. Note that the two series are independent from each other except for their equal averages.

[31] In contrast to applying a constant correction for a mean value, which would give correlations of 0, we find reasonable correlations for morning and noon, with rank correlations of 0.51 and 0.68, respectively. The evening series shows lower correlations of 0.28 and a rather small spread of the physics-based corrections. This is not surprising, since at the time of the evening measurement (20:00) no short-wave radiation is incident on the screen or sensor; hence, the corrections from our model depend on the long-wave radiation budged, which varies less than the short-wave budget. Note that the Δp evening series shows a similar and large spread (see Figure 4, right) for all cloudiness conditions.

[32] Figure 5 shows histograms for the morning, noon, and evening series of the $\Delta p_{i\in H3\ j}$ series and the $\Delta e_{p\ i\in H3\ j} - \Delta p_{i\in H3\ j}$ series (i.e., the differences after correction).

[33] The distributions of the $\Delta e_{p\ i\in H3\ j} - \Delta p_{i\in H3\ j}$ series are narrower than the $\Delta p_{i\in H3\ j}$ series for all three observation times (Figure 5, top) and centered on zero (Figure 5, bottom). Note, the application of a constant correction for the mean would just shift the whole distribution, higher-order distribution parameters would not be affected.

4.2. Correction Amounts and Impact of Physics-Based Corrections on Extreme Temperatures

[34] For correcting the Wild temperature series before the break, we use the statistically estimated $\overline{\Delta r_j}$ values as model constraints (equation (4)) and obtain individual correction magnitudes for every single sub-daily temperature value $\Delta e_{r\ i\in H2\ j}$. The corresponding estimated model parameters are presented in Table 2 in the last column.

[35] The (e.g. instrumental) offset c_0 derived from $\overline{\Delta r_j}$ is much larger than c_0 from $\overline{\Delta p_j}$. Δc_2 is almost identical, Δc_1 differs more, indicating potential problems in determining physically consistent coefficients (although the actual corrections are almost identical). No information is available from the station history about whether the same instrument was used in the Wild screen and after the screen change in the Stevenson screen. The estimated model parameter c_0 yields an offset of 0.8°C. This suggests either a change in instruments or an offset due to small changes in the station location (or instrument height), which in complex terrain may introduce an offset. Because of the possibility of an instrument change, we cannot use $\overline{\Delta p_j}$ for obtaining final corrections, but have to rely on $\overline{\Delta r_j}$.

[36] Figure 6 shows the physics-based corrections $\Delta e_{r\ i\in H3\ j}$ versus the $\Delta p_{i\in H3\ j}$ series, over the common interval when parallel measurements were taken. Δe_r and Δp show rank correlations of 0.71 and 0.45, for the noon and the morning series, respectively, but low correlations (0.16) for the evening series. In general, we find similar correlations as for the corrections derived from $\overline{\Delta p_{i\in H3\ j}}$ in Figure 4.

[37] Figure 7 (top) presents 3D scatterplots of the resulting correction magnitudes for the whole period before the break, *H*2, depending on the two radiation terms. There are notable clusters due to the categorical classes of the variables cloud cover and wind speed. For noon, the error magnitudes are clearly increasing with radiation, and the sign of the error is mostly negative. For morning, the corrections are positive for low radiation fluxes and get negative at higher radiation. In the evening, at all times net radiation on the surface of the screen is negative due to the missing short-wave radiation at 20:00; corrections are positive.

[38] Figure 7 (bottom) shows scatterplots of the physics-based corrections in *H*2 depending on temperature and wind speed. We find, in general, decreasing corrections at higher wind speeds, and larger corrections at increasing temperatures. However, at noon large corrections are also found on snow covered days with very low temperatures.

[39] Large ground albedo heavily increases reflected short-wave radiation. In contrast to the Stevenson screen, the sensor in the Wild screen is directly exposed to this enhanced radiation flux, which is accounted for in the correction model. Due to the dependence on radiation, the physics-based corrections in general show an annual cycle.

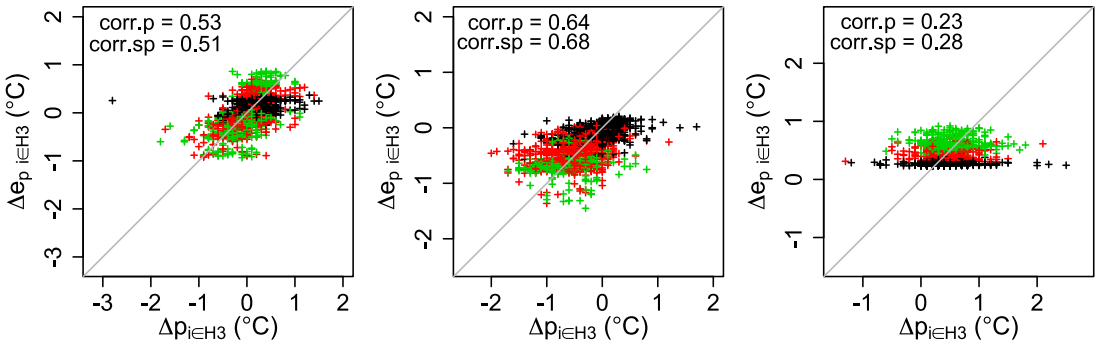

Figure 4. Physics-based corrections (calculated), $\Delta e_{p\ i\in H3\ j}$ versus differences from the parallel measurements (observed), $\Delta p_{i\in H3\ j}$, for (left) morning, (middle) noon, and (right) evening. Pearson (*corr. p*) and Spearman correlations (*corr.sp*) are indicated. Green symbols represent clear-sky, red partly cloudy, and black fully covered conditions.

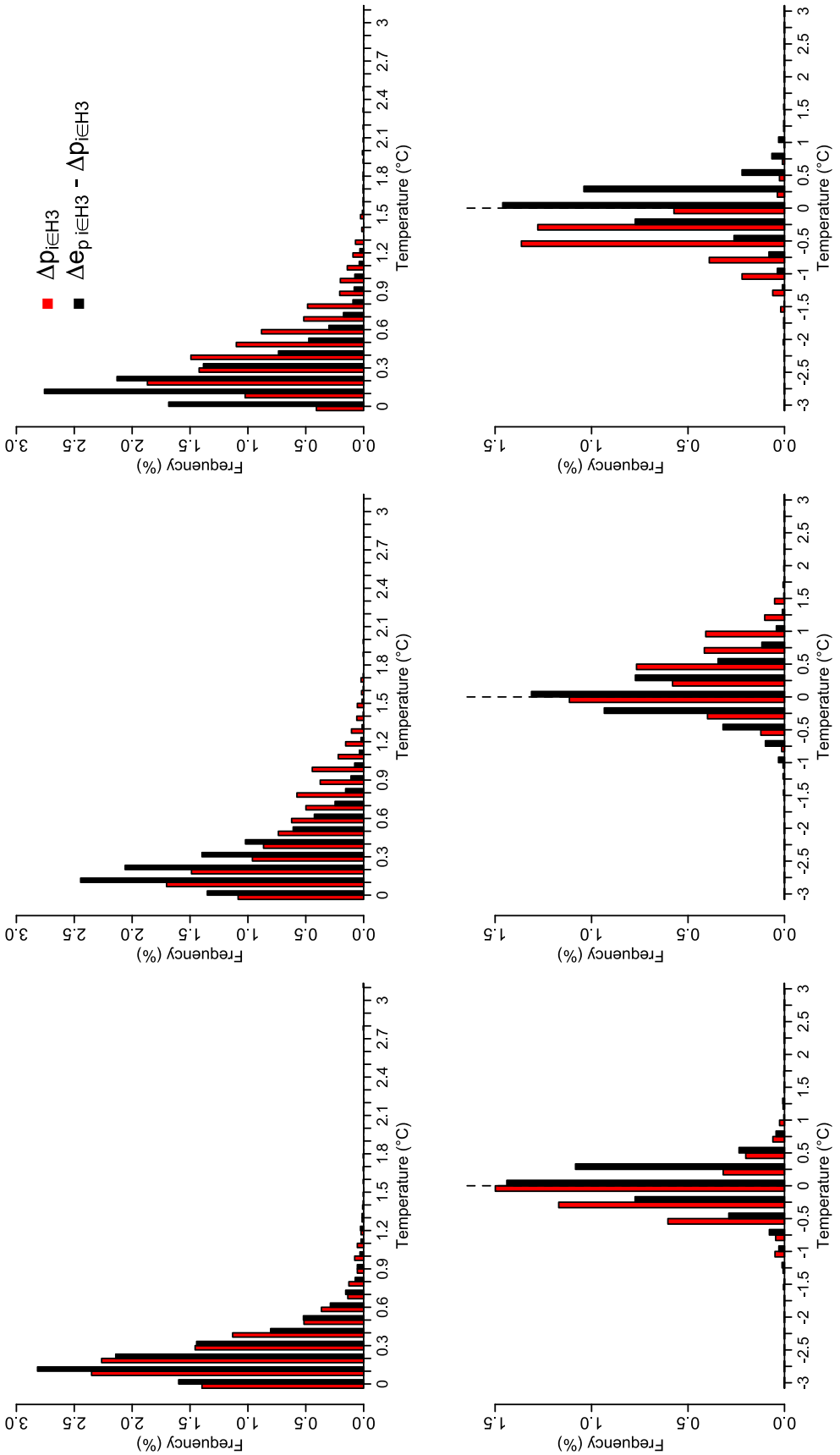

Figure 5. Histograms of the $\Delta p_{i \in H3\ j}$ series (red) and the $\Delta e_{p\ i \in H3\ j} - \Delta p_{i \in H3\ j}$ series (black) for (left) morning, (middle) noon, and (right) evening. (top) Absolute values. (bottom) Actual values.

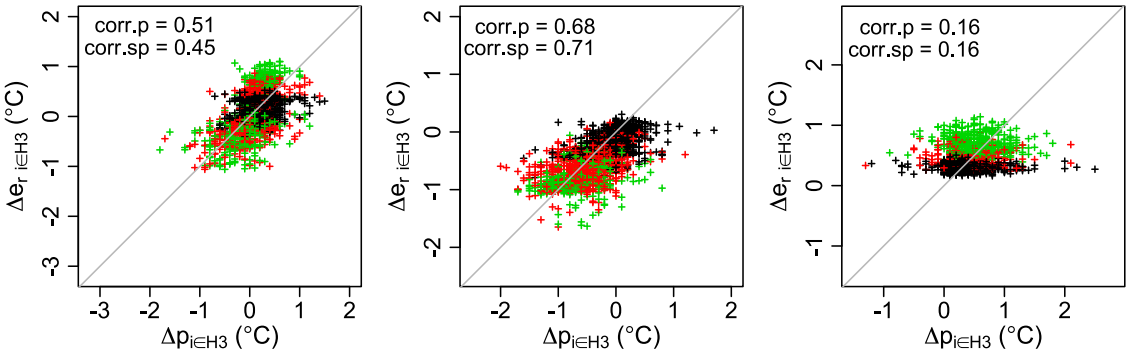

Figure 6. Physics-based corrections (calculated), $\Delta e_{r\ i\in H3\ j}$ versus differences from the parallel measurements (observed), $\Delta p_{i\in H3\ j}$ in the period *H3*, for (left) morning, (middle) noon, and (right) evening. Pearson (*corr.p*) and Spearman correlations (*corr.sp*) are again indicated. Green symbols represent clear-sky, red partly cloudy, and black fully covered conditions.

[40] Figure 8 presents the corrections as a function of the day of the year for different cloud cover classes (top row), and for different ground albedo classes (bottom row). On clear days with significant short-wave radiation (summer mornings, noon all year) and calm conditions, corrections are strongest negative. For all three observation times, fully covered days show the smallest corrections (around zero). In spring, there is a notable change in signs of the corrections for the morning measurements. This corresponds to the time when the sun is already above the local horizon at the time the measurement is taken, and the short-wave radiation components in the model are addressed. In Figure 8, our approach can be directly compared to daily corrections derived from interpolation from monthly or annual means.

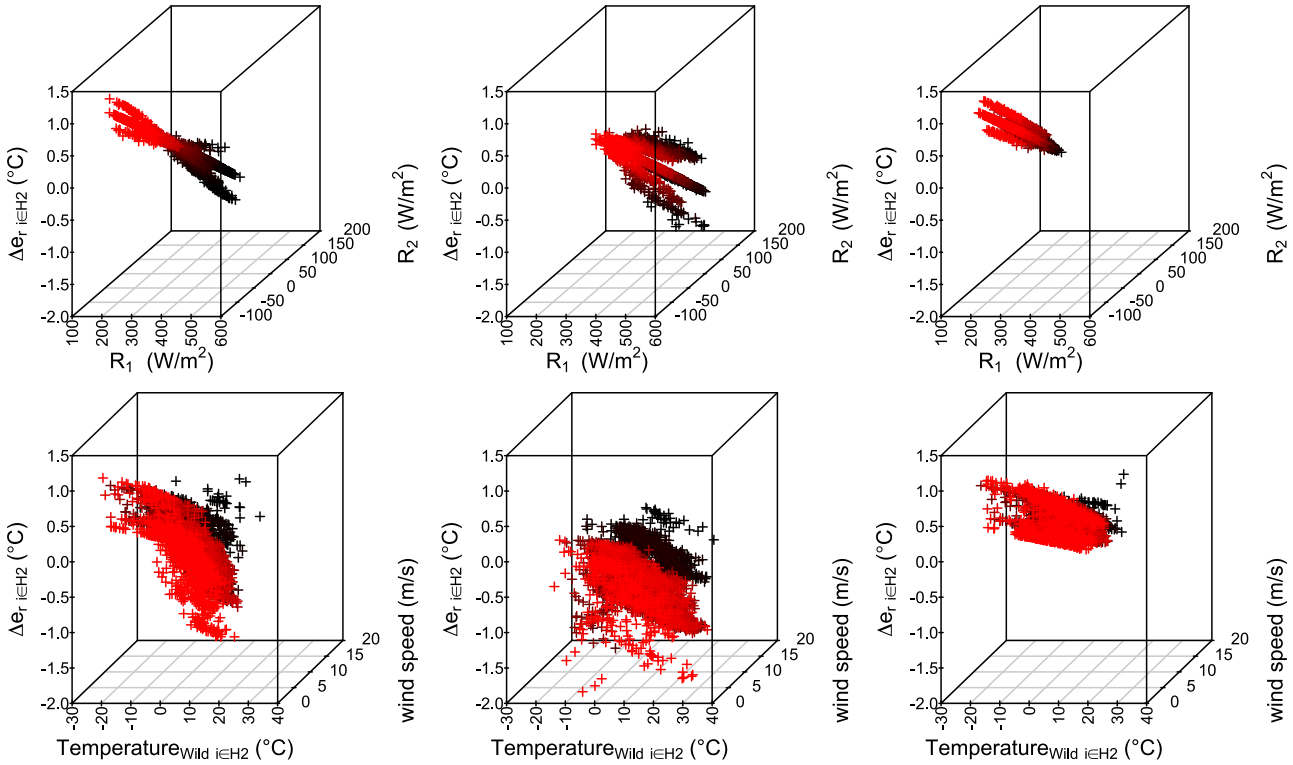

Figure 7. (top) Three-dimensional scatterplots with the physics-based corrections $\Delta e_{r\ i\in H2\ j}$ on the z-axis and radiation flux on the sensor and net radiation on the screen surface on the x- and y-axis, respectively. Red symbols denote lower R_2 values, black symbols higher R_2 values. Note that R_1 represents incoming radiation in contrast to R_2 representing net radiation. R_1 is therefore much larger. (bottom) Three-dimensional scatterplots with $\Delta e_{r\ i\in H2\ j}$ depending on temperature and wind speed, on the x- and y-axis, respectively. Red symbols denote low wind speeds, black symbols high wind speeds. One point in the bottom right panel (*wind speed* = 35 m/s, $Temperature_{Wild\ H2}$ = 11.3°C, $\Delta e_{r\ H2}$ = 0.3°C) is not shown due to graphical reasons. Results are presented for (left) morning, (middle) noon, and (right) evening.

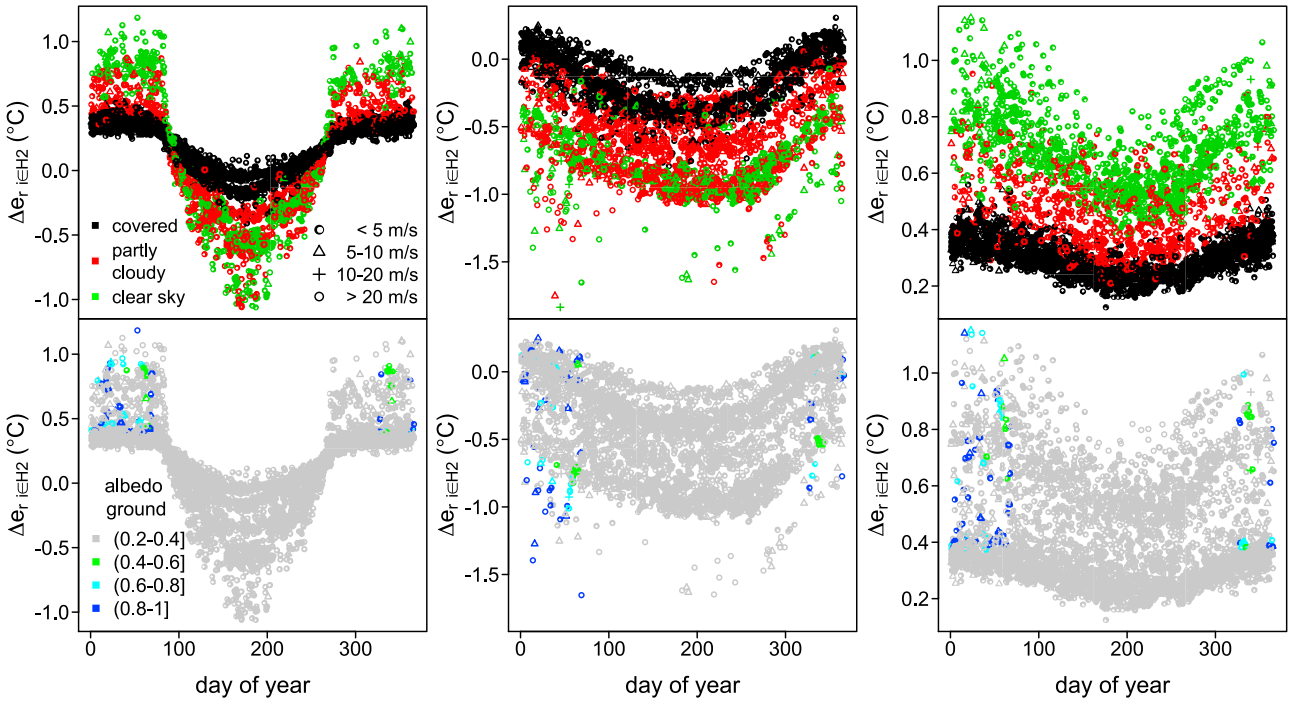

Figure 8. Physics-based derived corrections $\Delta e_{r\ i\in H2\ j}$ for (left) morning, (middle) noon, and (right) evening are presented as a function of the day of the year. Symbol colors in the top row denote different cloud cover classes (black for covered, red for partly cloudy, and green for clear sky). The different symbols indicate different wind speed classes for all six panels (see legend in top left panel). The symbol colors in the bottom row indicate different albedo classes (see bottom left panel for legend).

This approach would not show any spread in the corrections across the year (due to the nature of the method).

[41] We examine further the change in the sub-daily temperature distributions by comparing the uncorrected and corrected temperature series in *H*2 with the temperature series after the break in *H*1. Means and standard deviations are calculated and compared using the *t* and *F* test, respectively. Results are presented in Table 3.

[42] Temperature series before the correction are significantly different for the morning series (*Std dev*) and the evening series (*Mean*). Due to the nature of the method after correction, there are no significant differences for the mean; however, there are also no significant differences in the standard deviations. Repeating the same statistics, but using the respective difference series to the reference series gives similar results and reveals a significant reduction of variance due to the correction, although when compared to the statistics of the target difference series in *H*1 some significant differences in variances remain (not shown).

[43] To analyze the impact of the adjustments on extreme temperatures, the average number of days per year exceeding various temperature thresholds is given in Table 4 for the uncorrected series ($T_{Wild\ H2\ j}$), the series corrected for a mean shift ($T_{Wild\ H2\ j} + \overline{\Delta r_j}$), the physics-based corrected series ($T_{correction\ H2\ j}$), the Stevenson series during the period of parallel measurements ($T_{Stev\ H3}$), and the temperature series after the break ($T_{Stev\ H1\ j}$). Noon, morning, and daily mean temperatures are analyzed. T_{mean} was calculated according to contemporary standards using $(T_{morn} + T_{noon} + 2 * T_{eve})/4$.

Table 3. Mean and Standard Deviation (°C) for the Wild (Uncorrected) and Physics-Based Corrected Series in *H*2, and the Stevenson Series From the Most Recent Period *H*1

	$T_{Wild\ H2}$		$T_{corrected\ H2}$		$T_{Stev\ H1}$	
	Mean	Std Dev	Mean	Std Dev	Mean	Std Dev
Morning	7.3	7.5[a]	7.5	7.2	7.5	7.0
Noon	13.2	9.0	12.8	8.7	12.8	8.7
Evening	8.6	7.3[a]	9.1	7.2	9.1	7.2

[a]Significant difference between the uncorrected Wild (*H*2) and the Stevenson series (*H*1) or between the corrected series (*H*2) and the Stevenson series (*H*1) at the 0.05 level.

Table 4. Day-Count Indices (Average Number of Days per Year) for the Uncorrected Series ($T_{Wild\ H2}$), the Series Corrected for the Mean Shift ($T_{Wild\ H2} + \overline{\Delta r_{i\in H2}}$), the Physics-Based Corrected ($T_{corrected\ H2}$) Series, the Stevenson Series During the Period of Parallel Measurements ($T_{Stev\ H3}$), and the Stevenson Series After the Break ($T_{Stev\ H1}$)

	T_{noon}		T_{morn}		T_{mean}	
	>25°C	>30°C	<−10°C	<−15°C	>20°C	>25°C
$T_{Wild\ H2}$	33.2	6	6.4	1.5	24.1	1.1
$T_{Wild\ H2} + \overline{\Delta r_{i\in H2}}$	29.2	4.7	6.4	1.4	26	1.2
$T_{corrected\ H2}$	27.5	3.4	5.7	1.2	23.6	0.9
$T_{Stev\ H3}$	28.0	3.3	3.2	0.5	23.3	1
$T_{Stev\ H1}$	27.6	2.8	2.4	0.6	22.8	0.8

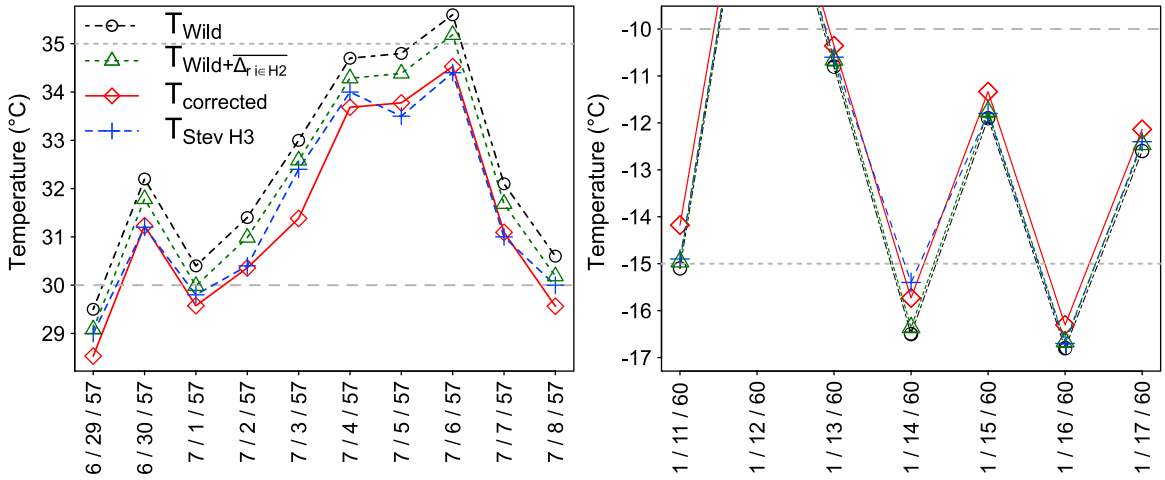

Figure 9. Comparison of the uncorrected series ($T_{Wild\ j}$), the series corrected for a mean shift ($T_{Wild\ j} + \overline{\Delta r_{i \in H2\ j}}$), the physics-based corrected series ($T_{corrected\ j}$), and the parallel measurements in the overlapping period ($T_{Stev\ j}$) during (left) a period of consecutive hot days in the beginning of July 1957 for the noon temperature series and (right) a period of consecutive very cold days in January 1960 for the morning temperature series.

For noon and morning, the uncorrected temperature series yields the highest number of days exceeding the extreme temperature thresholds, positive and negative. The average number of days decreases for the mean adjusted series, decreases even more for the physics-based adjusted series, and the temperature series in *H*3 and H1 (note *H*3 and *H*1 comprise a shorter period). The average annual number of days with mean daily temperatures exceeding 20°C and 25°C is highest for the mean shift corrected series and second largest for the uncorrected series. Again, the physics-based corrected series, the Stevenson series during the period of parallel measurements, and the Stevenson series after the break show very similar results as well as the smallest numbers of average exceedance days per year.

[44] Our findings are in accordance with the studies by *Z'graggen* [2006] and *Della-Marta and Wanner* [2006], who homogenized the 1966 break in Basel in the daily maximum temperature series. They also find a reduction of positive extremes following their corrections after the screen change.

[45] We further examined how the corrections affect temperatures in the hottest period at noon (Figure 9, left) and the coldest period in the morning series (Figure 9, right) from the six-year period with common parallel measurements. For the hot period (eight consecutive days with noon temperatures above 30°C), physics-based corrections yield between −0.7 and −1.7°C. We find remarkably good agreements with the parallel measurements. Compared to the mean shift corrected values (Figure 9, left, green triangles), the physics-based derived corrections are clearly larger in this period. Especially for days with extreme positive temperatures, mean adjustments may not be appropriate.

[46] In the cold period of consecutive days with morning temperatures mostly below −10°C, the agreement of the corrections with the parallel measurements is less pronounced as for the hot period. The physics-based corrections are generally positive, which is in accordance with the parallel measurements. Corrections in this period are smaller than +1°C, however being largest on clear sky days and partly cloudy days (due to the larger negative radiation balance), on 11th and 14th/15th, respectively.

5. Concluding Remarks

[47] A physics-based technique for correcting inhomogeneities present in sub-daily temperature records is proposed. It is introduced using the case of a specific inhomogeneity, namely the change from a Wild screen to the Stevenson screen. The method implies the distribution of a calculated mean annual error to single measurements based on environmental conditions at the time of measurement that affect the energy balance of the sensor-screen system (i.e., radiation and ventilation).

[48] The corrections lead to an improvement in the sub-daily temperature series, measured in the form of a decrease in the variance of the difference to independent parallel measurements. When comparing corrected and uncorrected series before and after the break, we find standard deviations of the uncorrected series before the break (morning 7.5°C, noon 9.0°C, evening 7.3°C) to be significantly different for the morning and evening temperatures from the series after the break (morning 7.0°C, noon 8.7°C, evening 7.2°C). After correction, the differences are not significant anymore (morning 7.2°C, noon 8.7°C, evening 7.2°C). The analyses of extreme temperatures demonstrate the importance of sub-daily correction for analyzing extremes, when the difference between different methods produces temperature differences in excess of 1°C. Comparing the average number of days per year exceeding a certain temperature threshold to parallel measurements shows a remarkable improvement in the corrected series. For noon temperatures exceeding 30°C, we find on average 3.3 days per year in the parallel measurements, compared to 6 days in the uncorrected series. After correction, the number decreases to 3.4 days.

[49] Our method requires a crude understanding of the error and at least annually resolved reference series. The

proposed model provides a valuable approach in addition to widely used, purely statistical corrections.

[50] The corrections derived from the physics-based model depend on various meteorological observations and measurements, which may introduce additional errors. Physical properties of the environment, especially wind speed, can vary even within small areas and short time periods. Obstacles and small variations in topography can influence environmental conditions in that even the same general atmospheric conditions can lead to different ventilation properties at a nearby site. The corresponding systematic error cannot be assessed. In addition, the transferability of the coefficients (e.g., whether the same coefficients can be used in one climatic region), and the robustness of the determination of coefficients needs to be explored. Identifying further existing parallel measurements and their accessibility will be a substantial task for future research on physical properties of inhomogeneities.

[51] Although designed for a specific cause of inhomogeneity, the model structure is general enough to be applied to other stations and situations. Moreover, the proposed model may be helpful as an error model, e.g., in the framework of data assimilation or for constructing benchmark data sets.

Appendix A: Radiation Model

[52] We introduce a simple radiation model for approximating net radiation on the surface of a Wild radiation screen (R_2) and incoming radiation on the temperature sensor (R_1). The following formulations of the particular radiative components are valid for approximating R_2 and R_1 and will be given in the following. Note that R_2 and R_1 represent net radiation and incident radiation flux, respectively. They further differ by their viewing geometries, which is accounted for with view factors (detailed at the end of this section).

[53] Radiative balance for an object can be split into solar (S) and thermal (L) radiation, as well as incoming (subscript *in*) and outgoing (subscript *out*). Net radiation (Q^*) thus reads:

$$Q^* = S_{in} - S_{out} + L_{in} - L_{out}. \tag{A1}$$

[54] In the short-wave spectrum, we account for direct (S_p) and diffuse radiation (S_d) from the atmosphere and reflected solar radiation from the ground (S_r) [*Campbell and Norman*, 1998].

$$S_{in} = S_p + S_d + S_r. \tag{A2}$$

[55] To quantify S_p we adapted the formulation of *Bonan* [2002]:

$$S_p = (1 - c)\ S_{p0}\ \tau^m \cos(\psi), \tag{A3}$$

where c is the cloud cover fraction (in tenths), S_{p0} is the extraterrestrial flux density perpendicular to the beam (W/m^2), τ is the transmissivity of the atmosphere, m is the optical air mass number, and ψ is the solar zenith angel (degrees). To account for cloud-covered conditions we scale S_p by the cloud-free fraction of the sky, hence assuming a linear relationship between S_p and the cloud cover fraction. The optical air mass number, m, is a relative measure that accounts for the difference in path length from a light source (sun) to sea level at different solar elevations expressed as a multiple of the path length at zenith ($m = 1$). The longer the path through the atmosphere, the larger the airmass and hence the attenuation of sunlight through scattering and absorption. We adopt a formulation for m that also accounts for refraction at high solar zenith angles [*Kumar et al.*, 1997; *Kreith and Kreider*, 1978]:

$$m = \left(1229 + (614 * \sin(90 - \psi))^2\right)^{0.5} - 614 * \sin(90 - \psi) * \frac{P_a}{P_0}, \tag{A4}$$

where ψ is the solar zenith angle (degrees), P_a is the pressure at the station (Pa), and P_0 is mean sea level pressure (Pa).

[56] For the fraction of sky diffuse radiation S_d, we adapt an empirical equation from *Liu and Jordan* [1960] :

$$S_d = 0.3\ (1 - (cmf\ \tau)^m)\ S_{p0}\ \cos\psi, \tag{A5}$$

where S_d is diffuse radiation, *cmf* is a cloud modification factor, and c is fractional cloud cover.

[57] Reflected radiation S_r is calculated as the product of the surface albedo (α_{ground}) and global radiation ($S_p + S_d$) on a horizontal surface:

$$S_r = \alpha_{ground}(S_p + S_d), \tag{A6}$$

where α_{ground} depends on the surface characteristics and differs considerably for grass and snow cover. As snow data are available for a very limited number of sites only, we set up a simple snow-accumulation model (see Appendix B) yielding daily ground albedo values.

[58] Outgoing short-wave radiation S_{out} is calculated by

$$S_{out} = S_{in}\ \alpha_{screen}, \tag{A7}$$

where α_{screen} is the albedo of the screen in the short-wave band.

[59] Incoming thermal radiation (L_{in}) comprises

$$L_{in} = L_a + L_g \tag{A8}$$

where L_a is the long-wave radiation from the atmosphere and L_g is thermal radiation emitted by the ground.

[60] L_a from the clear fraction of the sky ($L_{a,clear}$) is calculated as

$$L_{a,clear} = (1 - c)\epsilon_a \sigma T_a^4, \tag{A9}$$

where c is the cloud-covered sky fraction (in tenths), ϵ_a is the emissivity of the atmosphere, σ is the Stefan-Boltzmann constant, and T_a is the air temperature near the ground (K). ϵ_a is [*Brutsaert*, 1975]:

$$\epsilon_a = 1.24\left(\frac{\phi/100 e_s}{T_a}\right)^{1/7} \tag{A10}$$

where ϕ is the relative humidity and e_s is the saturation water vapor pressure, which was calculated after the formulation of *Bolton* [1980].

[61] We finally compute outgoing thermal radiation L_{out}:

$$L_{out} = \epsilon_{screen}\sigma T_a^4, \tag{A11}$$

Table A1. Sky View Factors for the Station Basel-Binningen

	S_d	S_r	L_g	L_a
F_{sensor}	0.4	0.6	0.6	0.4
F_{screen}	0.4	0.6	0.6	0.6

where ϵ_{screen} is the emissivity of the screen in the long-wave band (0.9 for a wooden object [*Brewster*, 1992; *Myers*, 2006]).

[62] To account for the different exposition of the screen and the sensor to the radiative components, components are multiplied by corresponding sky view factors (F) [*Campbell and Norman*, 1998]. We approximate the shape of the north-facing Wild screen as a cuboid (opened to the north and to the bottom) with a rectangular surface area (width = 1 m × height = 0.5 m × depth = 0.5 m) and assume the thermometer is located in the middle of the screen. For direct solar radiation on the screen surface, the view factor is expressed as the ratio of the screen area perpendicular to the beam, to the overall surface of the screen, depending on the zenith angle and azimuth. For non-directional components (diffuse and reflected short-wave and long-wave radiation), the fraction of the emitting hemisphere (ground or atmosphere), which is "seen" by the sensor or the outer surface of the screen, is used as the sky view factor. Hence, the maximum value of any sky view factor is 1. Due to the geometry of the Wild screen, the view factors for the sensor and the screen surface yield the values summarized in Table A1.

Appendix B: Snow-Accumulation Model

[63] The snow-accumulation model is based on the degree-day method [*Singh and Singh*, 2001], where temperature is used as an index for snowmelt. As input, we use maximum and minimum temperatures and daily water-equivalent or precipitation sums. First, we calculated the water-equivalent of daily new snow by simply assuming that the amount of water-equivalent does fall as snow when the daily mean temperature, calculated from the average of the morning and noon temperatures, is below 0°C. As we have no information on temperatures during the precipitation event, we use equal weighting of the minimum and maximum temperatures for the calculation. The definition of a degree-day (day on which snowmelt is prevalent) is based on the calculation of an index of temperature for snowmelt. Various methods may be used for deriving index temperatures (e.g., index temperature based on the 24-hourly mean temperature, on weighted averages of the minimum and maximum temperature, on maximum temperature only). We computed the index temperature from the average of the morning measurement plus twice the noon measurement, and determine a day exceeding the threshold of 1°C [*U.S. Army Corps of Engineers*, 1956; *Singh and Singh*, 2001] as a degree-day. We chose this calculation to account for the higher weights of the maximum temperature proposed by *Singh and Singh* [2001], which accounts for the effect of very low minimum temperatures dropping the temperature index below zero although daytime conditions might be (partly) adequate for snowmelt.

[64] For the degree-day factor for snow in Basel, which reflects the melting rate, we adapted a value of 1.74 *mm*/°C *day*, which was empirically found by the *U.S. Army Corps of Engineers* [1956] for similar regions and is in the range of the finding of *Gartska* [1964]. We take the degree-day factor as constant throughout the season, which is not necessarily the case. However, for our purpose this represents a sufficiently good approximation, as our aim is to estimate the dates with snow cover and not to reconstruct exact snow heights.

[65] To account for changing snow properties over time and as a consequence for changing snow albedo [*Wiscombe and Warren*, 1980], we applied a daily albedo-decreasing rate [*Singh and Kumar*, 1996] for consecutive days without fresh snow. We adapt the equation of *Eggleston et al.* [1971]

$$\alpha_s = r * (1 + \exp(-0.2 * (d_s - 1))) \quad \text{(B1)}$$

for albedo of aging snow (α_s), where d_s is the number of consecutive days of closed snow cover after fresh snow fall. The maximum albedo for fresh snow cover is set to a value of 0.7 (with r set to 0.35; for deep mountainous snowpacks r = 0.41 resulting in a maximum snow albedo of 0.82 [*Singh and Singh*, 2001]). We assume a rather low albedo because of possible impurities in the snow, decreasing snow albedo with cloud cover at low zenith angles [*Wiscombe and Warren*, 1980], neglecting the snowpack height, possible shadowing effects, and especially various other installed equipment and buildings on the ground.

[66] For the model, we used suitable model parameters from literature however, when a sufficiently long period is available, parameters can be calibrated. A validation of the modeled dates with snow cover from our model with a ten-year period of snow-height measurements in Basel (1956–1965) shows reasonable results. The dates of 70% of all observed snow covered days in this period could be reproduced by our model. For days without snow cover, an albedo of 0.25 (for grass [*Campbell and Norman*, 1998]) is used.

[67] **Acknowledgments.** We would like to thank Thierry Corti from the Center for Climate System Modeling (C2SM) and Victor Venema from the Meteorological Institute of the University of Bonn for helpful comments and Christine Füllemann, Michael Begert, and Mischa Croci-Maspoli from MeteoSwiss for discussions and information concerning data and homogenization, and for providing data and metadata. Thanks go to Franz Kuglitsch (University of Bern) for valuable discussions and comments. Furthermore, we would like to thank Max Baumann from the "Meteorologischer Verein" in Basel for providing the parallel measurements. The work was performed and funded under COST Action "HOME" and supported by NCCR Climate.

References

Aguilar, E., A. Moberg, D. Lister, and A. Walther (2008), A case-study/guidance on the development of long-term daily adjusted temperature datasets, *WMO/TD 1425*, World Meteorol. Org., Geneva, Switzerland.

Begert, M., M. Moesch, and P. Norm (2003), Homogenisierung von Klimamessreihen der Schweiz und Bestimmung der Normwerte 1961–1990, *Tech. Rep. 67*, MeteoSwiss, Zurich, Switzerland.

Begert, M., T. Schlegel, and W. Kirchhofer (2005), Homogeneous temperature and precipitation series of Switzerland from 1864 to 2000, *Int. J. Climatol.*, *25*, 65–80, doi:10.1002/joc.1118.

Bolton, D. (1980), The computation of equivalent potential temperature, *Mon. Weather Rev.*, *108*(7), 1046–1053.

Bonan, G. (2002), *Ecological Climatology*, 687 pp., Cambridge Univ. Press, Cambridge, U. K.

Brandsma, T., and G. P. Können (2006), Application of nearest-neighbor resampling for homogenizing temperature records on a daily to sub-daily level, *Int. J. Climatol.*, *26*(1), 75–89, doi:10.1002/joc.1236.

Brandsma, T., and J. P. van der Meulen (2008), Thermometer screen intercomparison in De Bilt (the Netherlands) Part II: Description and modeling of mean temperature differences and extremes, *Int. J. Climatol.*, *28*(3), 389–400, doi:10.1002/joc.1524.

Brewster, M. Q. (1992), *Thermal Radiative Transfer and Properties*, 568 pp., John Wiley, Hoboken, N. J.

Brönnimann, S. (2003), A historical upper air-data set for the 1939–44 period, *Int. J. Climatol.*, *23*(7), 769–791, doi:10.1002/joc.914.

Brutsaert, W. (1975), A theory for local evaporation (or heat transfer) from rough and smooth surfaces at ground level, *Water Resour. Res.*, *11*(4), 543–550, doi:10.1029/WR011i004p00543.

Campbell, G., and J. M. Norman (1998), *An Introduction to Environmental Biophysics*, 2nd ed., Springer, New York.

Corti, T., and T. Peter (2009), A simple model for cloud radiative forcing, *Atmos. Chem. Phys.*, *9*(15), 5751–5758, doi:10.5194/acp-9-5751-2009.

Della-Marta, P. M., and H. Wanner (2006), A method of homogenizing the extremes and mean of daily temperature measurements, *J. Clim.*, *19*(17), 4179–4197, doi:10.1175/JCLI3855.1.

Eggleston, K., E. Israelsen, and J. Riley (1971), Hybrid computer simulation of the accumulation and melt processes in a snowpack, technical report, Utah Water Res. Lab., Coll. of Eng., Utah State Univ., Logan.

Gartska, W. (1964), Snow and snow survey, in *Handbook of Applied Hydrology*, chap. 10, pp. 10.1–10.57, McGraw-Hill, New York.

Gates, D. (1980), *Biophysical Ecology*, 611 pp., Springer, New York.

Guttman, N. B., and C. B. Baker (1996), Exploratory analysis of the difference between temperature observations recorded by ASOS and conventional methods, *Bull. Am. Meteorol. Soc.*, *77*(12), 2865–2873.

Harrison, R. G. (2010), Natural ventilation effects on temperatures within Stevenson screens, *Q. J. R. Meteorol. Soc.*, *136*(646), 253–259, doi:10.1002/qj.537.

Hubbard, K., X. Lin, and E. Walter-Shea (2001), The effectiveness of the ASOS, MMTS, Gill, and CRS air temperature radiation shields, *J. Atmos. Clim.*, *18*(6), 851–864.

Huwald, H., C. W. Higgins, M.-O. Boldi, E. Bou-Zeid, M. Lehning, and M. B. Parlange (2009), Albedo effect on radiative errors in air temperature measurements, *Water Resour. Res.*, *45*, W08431, doi:10.1029/2008WR007600.

Kreith, F., and J. Kreider (1978), *Principles of Solar Engineering*, 232 pp., Hemisphere, New York.

Kuglitsch, F. G., R. Auchmann, R. Bleisch, S. Brönnimann, O. Martius-Romppainen, and M. Stewart (2012), Break detection of annual Swiss temperature series, *J. Geophys. Res.*, *117*, D13105, doi:10.1029/2012JD017729.

Kumar, L., A. Skidmore, and E. Knowles (1997), Modelling topographic variation in solar radiation in a GIS environment, *Int. J. Geogr. Inf. Sci.*, *11*(5), 475–497.

Lin, X., and K. Hubbard (2001), Radiation loading model for evaluating air temperature errors with a non-aspirated radiation shield, *Trans. ASAE*, *44*(5), 1299–1306.

Lin, X., K. Hubbard, and G. Meyer (2001), Airflow characteristics of commonly used temperature radiation shields, *J. Atmos. Oceanic Technol.*, *18*(3), 329–339.

Liu, B., and R. Jordan (1960), The interrelationship and characteristic distribution of direct, diffuse and total solar radiation, *Sol. Energy*, *4*(3), 1–19.

Mestre, O., C. Gruber, C. Prieur, H. Caussinus, and S. Jourdain (2011), SPLIDHOM: A method for homogenization of daily temperature observations, *J. Appl. Meteorol. Climatol.*, *50*(11), 2343–2358, doi:10.1175/2011JAMC2641.1.

Moberg, A., et al. (2000), Day-to-day temperature variability trends in 160- to 275-year-long European instrumental records, *J. Geophys. Res.*, *105*(D18), 22,849–22,868.

Moberg, A., et al. (2006), Indices for daily temperature and precipitation extremes in Europe analyzed for the period 1901–2000, *J. Geophys. Res.*, *111*, D22106, doi:10.1029/2006JD007103.

Müller, G. (1984), Vergleich der Temperaturen verschiedener Wetterhütten an einigen Stationen des ANETZ, *Arbeitsber. MeteoSchweiz*, *119*, 36 pp.

Myers, R. L. (2006), *The Basics of Physics*, 365 pp., Greenwood, Westport, Conn.

Nakamura, R. (2005), Air temperature measurement errors in naturally ventilated radiation shields, *J. Atmos. Oceanic Technol.*, *22*(7), 1046–1058, doi:10.1175/JTECH1762.1.

Nordli, P. Ø., H. Alexandersson, P. Frich, E. J. Førland, R. Heino, T. Jónsson, H. Tuomenvirta, and O. E. Tveito (1997), The effect of radiation screens on Nordic time series of mean temperature, *Int. J. Climatol.*, *17*(15), 1667–1681.

Oke, T. R. (1987), *Boundary Layer Climates*, 2nd ed., 435 pp., Methuen, New York.

Paltridge, C. W., and C. M. R. Platt (1976), *Radiative Processes in Meteorology and Climatology*, Elsevier, New York.

Peterson, T. C., and D. R. Easterling (1994), Creation of homogeneous composite climatological reference series, *Int. J. Climatol.*, *14*(6), 671–679.

Peterson, T., D. Easterling, and T. Karl (1998), Homogeneity adjustments of in situ atmospheric climate data: A review, *Int. J. Climatol.*, *18*(13), 1493–1517.

Raunio, N. (1950), Amendments to the computation of the radiation error of the Finnish (Väisälä) radiosonde, *Geophysica*, *4*, 14–20.

Richardson, S. J., F. V. Brock, S. R. Semmer, and C. Jirak (1999), Minimizing errors associated with multiplate radiation shields, *J. Atmos. Oceanic Technol.*, *16*(11), 1862–1872.

Singh, P., and N. Kumar (1996), Determination of snowmelt factor in the Himalayan region, *Hydrol. Sci. J.*, *41*(3), 301–310.

Singh, P., and V. P. Singh (2001), *Snow and Glacier Hydrology*, 742 pp., Kluwer Acad., Dordrecht, Netherlands.

Štěpánek, P., P. Zahradníček, and P. Skalák (2009), Data quality control and homogenization of air temperature and precipitation series in the area of the Czech Republic in the period 1961–2007, *Adv. Sci. Res.*, *3*, 23–26, doi:10.5194/asr-3-23-2009.

Stephens, G. L., S.-C. Tsay, P. W. Stackhouse, and P. J. Flatau (1990), The relevance of the microphysical and radiative properties of cirrus clouds to climate and climatic feedback, *J. Atmos. Sci.*, *47*(14), 1742–1754.

Toreti, A., F. G. Kuglitsch, E. Xoplaki, J. Luterbacher, and H. Wanner (2010), A novel method for the homogenization of daily temperature series and its relevance for climate change analysis, *J. Clim.*, *23*(19), 5325–5331, doi:10.1175/2010JCLI3499.1.

U.S. Army Corps of Engineers (1956), Snow hydrology summary report of the snow investigations, technical report, North Pac. Div., Portland, Oreg.

Väisälä, V. (1941), Der Strahlungsfehler der finnischen Radiosonde, *Mitt. Meteorol. Inst. Univ. Helsinki*, *47*(1), 63 pp.

Väisälä, V. (1949), Solar radiation intensity at the ascending radiosonde, *Geophysica*, *3*, 37–55.

van der Meulen, J. P., and T. Brandsma (2008), Thermometer screen intercomparison in De Bilt (The Netherlands). Part I: Understanding the weather-dependent temperature differences), *Int. J. Climatol.*, *28*(3), 371–387, doi:10.1002/joc.1531.

Venema, V. K. C., et al. (2012), Benchmarking homogenization algorithms for monthly data, *Clim. Past*, *8*(1), 89–115, doi:10.5194/cp-8-89-2012.

Vincent, L. A., X. Zhang, B. R. Bonsal, and W. D. Hogg (2002), Homogenization of daily temperatures over Canada, *J. Clim.*, *15*, 1322–1334.

Wiscombe, W. J., and S. G. Warren (1980), A model for the spectral albedo of snow. I: Pure snow, *J. Atmos. Sci.*, *37*(12), 2712–2733.

World Meteorological Organization (2008), Guide to meteorological instruments and methods of observation, *Tech. Rep. 8*, Geneva, Switzerland.

Z'graggen, L. (2006), Die Maximaltemperaturen im Hitzesommer 2003 und Vergleich zu früheren Extremtemperaturen, *Arbeitsber. MeteoSchweiz*, *212*, 74 pp.